

Kinematic and Microphysical Significance of Lightning Jumps
versus Non-Jump Increases in Total Flash Rate

CHRISTOPHER J. SCHULTZ *

Department of Atmospheric Science, The University of Alabama in Huntsville and NASA MSFC, Huntsville, Alabama

LAWRENCE D. CAREY

Department of Atmospheric Science, The University of Alabama in Huntsville, Huntsville, Alabama

ELISE V. SCHULTZ

Earth System Science Center, The University of Alabama in Huntsville, Huntsville, Alabama

RICHARD J. BLAKESLEE

NASA Marshall Space Flight Center, Huntsville, Alabama

* *Corresponding author address:* Christopher J. Schultz, UAH/NASA Marshall Space Flight Center, 320 Sparkman Drive, Huntsville, AL 35805.
E-mail: schultz@nsstc.uah.edu

ABSTRACT

Thirty-nine thunderstorms are examined using multiple-Doppler, polarimetric and total lightning observations to understand the role of mixed phase kinematics and microphysics in the development of lightning jumps. This sample size is larger than those of previous studies on this topic. The principal result of this study is that lightning jumps are a result of mixed phase updraft intensification. Larger increases in intense updraft volume ($\geq 10 \text{ m s}^{-1}$) and larger changes in peak updraft speed are observed prior to lightning jump occurrence when compared to other non-jump increases in total flash rate. Wilcoxon-Mann-Whitney Rank Sum testing yields p-values ≤ 0.05 , indicating statistical independence between lightning jump and non-jump distributions for these two parameters. Similar changes in mixed phase graupel mass magnitude are observed prior to lightning jumps and non-jump increases in total flash rate. The p-value for graupel mass change is $p=0.096$, so jump and non-jump distributions for graupel mass change are not found statistically independent using the $p=0.05$ significance level. Timing of updraft volume, speed and graupel mass increases are found to be 4 to 13 minutes in advance of lightning jump occurrence. Also, severe storms without lightning jumps lack robust mixed phase updrafts, demonstrating that mixed phase updrafts are not always a requirement for severe weather occurrence. Therefore, the results of this study show that lightning jump occurrences are coincident with larger increases in intense mixed phase updraft volume and peak updraft speed than smaller non-jump increases in total flash rate.

1. Introduction

Sudden increases in total flash rates are denoted as lightning jumps. Research about lightning jumps has primarily focused on the correlation between lightning jumps and severe weather¹ occurrence (e.g., Williams et al. 1999, Schultz et al. 2009, Gatlin and Goodman 2010, Schultz et al. 2011, Rudlosky and Fuelberg 2013). However, these studies lack analysis of the microphysical and dynamical mechanisms which lead to a rapid increase in total flash rate.

Several studies observed good correlation between total lightning trends and mixed phase ice mass or updraft volume, but poorer correlation between total lightning and maximum updraft speed over the entire lifecycle of thunderstorms (e.g., Workman and Reynolds 1949, Goodman et al. 1988, Tuttle et al. 1989, Dye et al. 1989, Carey and Rutledge 1996, Lang and Rutledge 2002, Wiens et al. 2005, Tessendorf et al. 2005, Kuhlman et al. 2006, Deierling et al. 2008, Deierling and Petersen 2008). These studies relied on the observed connection between kinematics, microphysics and electrification within thunderstorms via the non-inductive charging mechanism (e.g., Takahashi 1978, Saunders et al. 2006).

Electrification within thunderstorms is found to occur on the order of the quarter to half life of a ordinary thunderstorm². Research shows that initial electrification in the primary development of thunderstorms is approximately 10-15 minutes (e.g., Dye et al. 1986, Bringi et al. 1997). Lightning jumps themselves also occur on timescales which are on the order of several minutes (Goodman et al. 1988, Williams et al. 1989, Williams et al. 1999). Therefore, storm properties that are well-correlated to total flash rate on longer timescales may

¹Defined as the presence of hail ≥ 2.54 cm, winds ≥ 26 m s⁻¹ or a tornado.

²The duration of an ordinary thunderstorm is 30-60 minutes (Byers and Braham 1949).

not represent the same mechanisms which result in lightning jumps.

Schultz et al. (2015) examined the correspondence between lightning jumps and trends in mixed phase graupel mass, maximum updraft speed and updraft volume on 15 minute time scales for 4 thunderstorms of varying morphology. These specific parameters were chosen because of their strong correlations to total flash rate from studies mentioned previously in this paper. Schultz et al. (2015) showed that lightning jumps occur when the 10 m s^{-1} updraft volume and mixed phase graupel mass increase prior to jump occurrence. They also determined that maximum updraft speed increases in 8 of the 12 flash rate periods examined. However, Schultz et al. (2015) did not robustly demonstrate how the kinematic and microphysical mechanisms examined differ between lightning jumps and other non-jump increases in total flash rate because of a small sample size.

Therefore, the goal of this research is to determine whether there are statistically significant differences between lightning jumps and non-jump increases in total flash rate using a large sample of thunderstorm observations. Analysis of the kinematic and microphysical characteristics will assess if larger changes in the magnitude of mixed phase graupel mass, updraft volume or maximum updraft speed occur prior to lightning jumps versus other non-jump increases in total flash rate. This analysis will also evaluate the temporal correspondence between the 2σ lightning jump algorithm (Schultz et al. 2009, Schultz et al. 2011, Schultz et al. 2015) and the underlying kinematic and microphysical thunderstorm characteristics needed for rapid electrification. The 2σ algorithm is currently being used experimentally at the National Oceanic and Atmospheric Administration’s Hazardous Weather Testbed (NOAA HWT; Calhoun 2015) in preparation for the launch of GOES-R’s Geostationary Lightning Mapper (GLM; Goodman et al. 2013).

2. Data and Methods

The data, study domain³ and analysis methods are similar to those of Schultz et al. (2015) for continuity between the results of that study and the present study. The focus is using total lightning, polarimetric and multi-Doppler data and analysis to characterize kinematic and microphysical changes within a thunderstorm prior to any increase in total flash rate. This research provides more comprehensive statistical metrics related to the physical mechanisms hypothesized to modulate electrification and lightning production within thunderstorms.

A total of 39 thunderstorms are used in this analysis. Convective intensity of the thunderstorms examined ranges from weak ordinary multicellular convection and low-topped winter convection to bowing segments within quasi-linear convective systems (QLCS) and supercells (Table 1). Of the 39 thunderstorms, 20 thunderstorms contain at least 1 lightning jump, and 19 possess zero lightning jumps while they are within the multi-Doppler domain. Twenty-three of the 39 thunderstorms are multicellular thunderstorms, 10 thunderstorms are supercells, 3 are low topped supercell storms, 2 are bowing segments within QLCSs and 1 storm is in the outer bands of a remnant tropical cyclone. In total, 214-fifteen minute analysis periods prior to an increase in total flash rate (both jumps and non-jump increases) are analyzed from these 39 thunderstorms. Properties which are examined in this analysis include: mixed phase graupel mass (-10° to -40°C), 5 and 10 m s^{-1} mixed phase updraft

³See Fig. 1 of Schultz et al. (2015).

92 volume, and maximum updraft speed.

93
94 *a. Radar Data*

95 The same radar data and methodologies used in Schultz et al. (2015) are employed in this
96 study. The University of Alabama in Huntsville’s (UAH) Advanced Radar for Operational
97 Research (ARMOR; Schultz et al. 2012, Knupp et al. 2014) and the National Weather
98 Service’s (NWS) radar located at Hytop, AL (KHTX; Crum and Alberty 1993) are used
99 for three-dimensional retrieval of velocity and bulk characterization of hydrometeor types
100 within thunderstorms. ARMOR can be taken out of its default 5 tilt operational mode to
101 collected higher temporal resolution and larger volumetric data for research purposes. All
102 radar data are corrected for attenuation and differential attenuation (Bringi et al. 2001).
103 Aliased velocities are unfolded using NCAR’s SOLO software (Oye et al. 1995) and ground
104 clutter, side lobe and second trip echoes are also removed from all radar data. Data are
105 gridded to a Cartesian coordinate system using a grid spacing of 1 km x 1 km x 1 km on a
106 grid of 300 km x 300 km x 19 km. This spacing is chosen because of the resolution limita-
107 tions of the longer baseline used for the ARMOR-KHTX domain (e.g., Davies-Jones 1979,
108 Deierling and Petersen 2008). A Cressman weighting scheme is implemented using 1 km
109 radius of influence centered at each grid point with NCAR’s REORDER software (Oye and
110 Case 1995). Individual thunderstorms are identified and semi-objectively tracked using the
111 Thunderstorm Identification Tracking Analysis and Nowcasting (TITAN; Dixon and Wiener
112 1993) algorithm to assign radar and lightning characteristics to individual storms. This

tracking method is the same used in previous lightning jump studies (Schultz et al. 2009, Schultz et al. 2011, Schultz et al. 2015).

The National Center for Atmospheric Research’s (NCAR) Custom Editing and Display of Reduced Information in Cartesian Space (CEDRIC; Mohr et al. 1986) is used to perform multi-Doppler synthesis. Vertical velocity retrievals are calculated using radial velocity measurements from two or more radars and a reflectivity based hydrometeor fall speed relationship to solve a set of linear equations (e.g., Armijo 1969, O’Brien 1970, Brandes 1977, Ray et al. 1980, Deierling and Petersen 2008, Schultz et al. 2015). Horizontal velocity components u and v derived from radial velocity measurements from both radars and are used to solve for the vertical velocity component (w) by integrating the anelastic continuity equation.

Similar to Schultz et al. (2015), the variational integration technique is utilized in this study to evaluate trends in updraft within thunderstorms (e.g., O’Brien 1970, Matejka and Bartels 1998, their Section 2e). The variational technique is chosen for this analysis for continuity between the methods used in this study and other studies using the ARMOR-KHTX baseline (e.g., Deierling and Petersen 2008, Johnson 2009, Mecikalski et al. 2015, Carey et al. 2016). The advantage of the variational integration technique is that it redistributes errors from both boundary conditions to produce profiles of vertical air motion and divergence that converge to a solution (O’Brien 1970, Matejka and Bartels 1998). The downward integration scheme could also be utilized for similar analysis of updrafts.

Vertical velocity is set at 0 m s^{-1} at the upper and lower bounds of integration (0 and 17 km). Integration of the anelastic mass continuity equation is performed from the upper and lower bounds of integration for all points within the multi-Doppler domain. Upward

integration is performed from 0 km up to 3 km and downward integration is performed from the upper boundary from 17 km down to (and including) 3 km. Upward integration is only used below 3 km because of potential errors introduced into the calculation of divergence and vertical velocity at low-levels from radar beam height limitations (i.e., radar data do not extend all of the way to the surface). However, updraft information used for analysis is limited to the -10° to -40°C , which is ≥ 4 km in the 39 cases examined and these levels utilize calculations from the downward integration of continuity. Integration of the anelastic continuity equation results in an estimate of vertical velocity for each 1 km^3 volume where u , v and divergence are calculated in the vertical column.

Analysis of updraft speed and volume are limited to the mixed phase region of the thunderstorm (i.e., between -10°C and -40°C isotherms) because the mixed phase region is where charge development and separation take place to ultimately lead to electrical breakdown (e.g., Dye et al. 1986, Carey and Rutledge 1996, Bringi et al. 1997, Deierling and Petersen 2008, Calhoun et al. 2013). Maximum updraft speed and a sum of 1 km^3 updraft volumes with speeds $\geq 5 \text{ m s}^{-1}$ and 10 m s^{-1} are computed from the multi-Doppler Cartesian grids for all multi-Doppler syntheses in which a thunderstorm is identified and tracked by TITAN. The longer baseline between the radars means that updraft values calculated in the study are smaller in magnitude than the true updraft observed if higher resolution observations were available. However, the trend in the updraft can still be characterized, especially with horizontal resolution $\leq 1.5 \text{ km}$ in the domain used in this study. This longer baseline approach is used in similar lightning/updraft studies like Deierling and Petersen (2008), Mecikalski et al. (2015) and Carey et al. (2016).

Particle identification is performed using ARMOR radar data and the NCAR Particle

Identification Algorithm (PID; Vivekanandan et al. 1999) modified for C-band observations (Deierling et al. 2008, Johnson 2009, Schultz et al. 2015) to identify the dominant scatterer observed in each ARMOR radar volume. Graupel/small hail category is the primary hydrometeor of interest in this study because of graupel’s strong tie to electrification and lightning production in thunderstorms through NIC processes (e.g., Carey and Rutledge 1996, Saunders et al. 2006, Deierling et al. 2008). Graupel mass is calculated using a z-M relationship of,

$$mass \ (g \ m^{-3}) = 0.0052 \times z^{0.5}, \quad (1)$$

from Heymsfield and Miller (1988). The letter z represents the reflectivity factor in linear units of $mm^6 \ m^{-3}$, and this calculation is made for each volume where graupel/small hail is identified to be the dominant particle in a $1 \ km^3$ volume. All $1 \ km^3$ between $-10^\circ C$ and $-40^\circ C$ that also fell inside the thunderstorm’s TITAN footprint are then used to calculate a total mass for the storm at each ARMOR radar volume time.

b. Lightning Data

The same lightning data and methods used in Schultz et al. (2015) are employed in this study. Total lightning information is collected by the North Alabama Lightning Mapping Array (NALMA, Koshak et al. 2004, Goodman et al. 2005). Very high frequency (VHF) source points are combined into corresponding flashes using a flash clustering algorithm developed by McCaul et al. (2009). This cluster algorithm requires that all VHF source points 0.3 s apart in time and that satisfy an azimuth and range dependent spatial separation re-

striction are grouped into a single lightning flash⁴. A flash must have a minimum of 10 VHF source points to be considered in this analysis.

1) THE LIGHTNING JUMP

The sigma-level configuration of the 2σ lightning jump algorithm is used to categorize jump and non-jump increases in total flash rate within this study (Schultz et al. 2009, Schultz et al. 2011). Sigma-level is represented by,

$$\text{sigma-level} = \frac{DFRDT_{t_o}}{\sigma(DFRDT_{t-2,t-4,t-6,t-8,t-10})}, \quad (2)$$

where $DFRDT_{t_o}$ represents the time rate of change of the total flash rate at the current time, and $\sigma(DFRDT_{t-2,t-4,t-6,t-8,t-10})$ represents the standard deviation of time rate of change for the previous 12 minutes of lightning data starting at $t - 2$. Please see Appendix A or Schultz et al. (2011), Chronis et al. (2015) and Schultz et al. (2015) for more detail on the calculation of the 2σ lightning jump algorithm. All increases in total flash rate (i.e., positive sigma-level) are examined, and flash rate increases are binned into two groups by their sigma-level. A non-jump increase in flash rate has a sigma-level <2 (hereafter defined as the 0-2 category) and a lightning jump has a sigma-level ≥ 2 (hereafter defined as the 2+ category).

⁴For more information on the spatial requirements, see McCaul et al. (2009) and references within the article.

c. *Analysis Windows*

Trends in updraft speed, updraft volume and graupel mass are determined in the following manner. First, the time of the flash rate increase (t_o) is used to identify radar volumes within ± 2 minutes of occurrence. If two radar volumes are available, the one closest to the time of the flash rate increase is used. Similarly, the closest radar volume to the time 15 minutes prior to the flash rate increase (i.e., $t-15$) is also identified. This radar volume also must occur within ± 2 minutes of the $t-15$ time. Next the local trend in each radar derived parameter is determined by subtracting the value at time $t-15$ from time t_o . The magnitude of the change is placed into the corresponding sigma-level category. A 15 minute analysis window is chosen because it is on the order of the quarter to half life of an ordinary thunderstorm (Byers and Braham 1949), its the approximate amount of time for the onset of electrification (Dye et al. 1986, Bringi et al. 1997) and this period allows for 2-3 radar updates from the WSR-88D radars to obtain trends in other intensity metrics like maximum expected size of hail (MESH; Witt et al. 1998) or azimuthal shear. Lengthening the analysis window could also incorporate data which is less likely to be attributed to the development of a lightning jump (Schultz et al. 2015).

d. *Statistical Significance*

Assessment of statistical independence between the jump and non-jump distributions is made for each kinematic or microphysical quantity in this study (i.e., mixed phase updraft volume, updraft speed or graupel mass). The Wilcoxon-Mann-Whitney Rank-Sum Test is

used to determine the degree of independence between the 0-2 and 2+ sigma-level data distributions for updraft volume, updraft speed and graupel mass (Wilks 1995, pp. 159-163). The use of the rank sum test is ideal for this dataset because the sampling distribution of the data is unknown and this test is resistant to any potential outliers. Z-scores and p-values for each of the comparisons are presented to illustrate the level of significance between the 0-2 and 2+ sigma-level categories. The null hypothesis is that the 0-2 and 2+ sigma-level are drawn from the same distribution for each parameter examined in this study. Thus, if the p-value is $p \leq 0.05$, the null hypothesis is rejected and the property is more likely observed with lightning jump occurrence than a general increase in flash rate. If the p-value is $p > 0.05$, the null hypothesis is supported and the kinematic/microphysical property is observed for any increase in total flash rate and not solely for lightning jumps.

3. Results

Parameters of mixed phase graupel mass, updraft volume and updraft speed are examined to determine differences in the kinematic and microphysical growth within a thunderstorm prior to lightning jumps and non-jump increases in total flash rate. Changes in these quantities in a 15 minute analysis window will help determine the degree to which well-correlated parameters observed in previous studies can differentiate between lightning jumps and non-jump increases in total flash rate. Ultimately, lightning jumps could be used to infer a higher likelihood that a specific physical process is present if a lightning jump is observed, especially for physical parameters which are not readily available (e.g., updraft speed, updraft volume).

239 *a. Mixed Phase Graupel Mass*

240 Growth of mixed phase graupel mass in this sample of thunderstorms is observed prior
 241 to the majority of total flash rate increases (Fig. 1). The median changes for the 0-2 and 2+
 242 sigma-level categories are 5.70×10^7 kg and 7.15×10^7 kg, respectively. There is considerable
 243 overlap of the inner quartile ranges (IQR) within each sigma-level category. Wilcoxon-Mann-
 244 Whitney Rank Sum testing illustrates that the two distributions are statistically similar
 245 (Table 2). The 0-2 and 2+ graupel mass distributions result in a Z-score of 1.065, with a
 246 one tailed p-value of 0.096. This p-value is larger than the $p=0.05$ value used to determine
 247 statistical independence, so the null hypothesis of similar distributions is supported, and
 248 larger increases in mixed phases graupel mass are not observed to statistically discriminate
 249 between lightning jump and non-jump increases in total flash rate⁵.

250

251 *b. Updraft Volume*

252 The change in mixed phase 5 m s^{-1} updraft volume also does not discriminate between
 253 lightning jump and non-jump increases in total flash rate. Small differences are observed
 254 in the distributions between the two sigma-level categories (Fig. 2A). Medians of the 0-2
 255 and 2+ sigma-level categories are 66 and 125 km^3 , respectively. Wilcoxon-Mann-Whitney

⁵These calculations only include volumes of the storm where graupel is identified as the dominant type of hydrometeor.

Rank Sum Testing shows that these two distributions are statistically similar Fig. 2A. The Z-score and p-value of 1.323 and 0.093 for 5 m s^{-1} updraft volume change supports the null hypothesis since the p-value is larger than the $p=0.05$ independence threshold. This result demonstrates that larger increases in 5 m s^{-1} updraft volume are not observed to statistically discriminate between lightning jumps and non-jump increases in total flash rate.

The change in mixed phase 10 m s^{-1} updraft volume prior to flash rate increases shows larger differences between the jump and non-jump categories. Median growth of the 10 m s^{-1} updraft volume in the 0-2 and 2+ sigma-level category is 16 and 62 km^3 , respectively (Fig. 2B). Wilcoxon-Mann-Whitney Rank Sum Testing demonstrates that the two distributions are different. The Z-score and p-value for 10 m s^{-1} updraft volume change are 1.987 and 0.0234 (Table 2). Thus, the null hypothesis is rejected for 10 m s^{-1} updraft volume, and larger increases in 10 m s^{-1} updraft volume are observed to statistically discriminate between lightning jumps and non-jump increases in total flash rate.

c. Peak Updraft Speed

Change in peak mixed phase updraft speed reveals a major difference in the distributions of the two sigma-level categories (Fig. 3). Medians of the 0-2 and 2+ sigma-level categories are 1 and 5 m s^{-1} from the $1 \text{ km} \times 1 \text{ km} \times 1 \text{ km}$ resolution data used in this analysis. Wilcoxon-Mann-Whitney Rank Sum Testing shows that the two populations are different in Fig. 3. The Z-score for the change in peak updraft speed is 3.286, with a p-value of 5.0×10^{-4} . This indicates that the null hypothesis of similar distributions for jump and non-jump in-

creases in total flash rate is rejected at the $p=0.05$ significance level (Table 2). Thus, a larger magnitude change in the mixed phase maximum updraft speed in a thunderstorm is more likely associated with the development of a 2σ lightning jump than non-jump increases in total flash rate.

d. Timing of Increases

Figure 4 shows the difference in time between the time of 0-2 and 2+ sigma-level increases in total flash rate and the maximum increase in each of the 3 parameters (graupel mass, 10 m s^{-1} updraft volume, maximum updraft speed). The time of the lightning increase is subtracted from the time of the peak increase in the 3 parameters to maintain a reference frame centered on the time of the lightning increase. In general, the largest increase in graupel mass, 10 m s^{-1} updraft volume and maximum updraft speed during each 15 minute analysis window is occurring on the order of 4 to 13 minutes prior to all increases in the total flash rate.

4. Discussion

a. The Importance of Peak Updraft Speed and 10 m s^{-1} Updraft Volume

Table 2 shows that the peak updraft speed is one of two parameters examined that demonstrates statistical independence between lightning jumps and non-jump increases in

flash rate (the other being 10 m s^{-1} updraft volume). Therefore, the maximum updraft is not necessarily well-correlated to the total flash rate over the entire lifetime of a thunderstorm, but the observations in this study indicate the increased likelihood that larger increases in maximum updraft speed are observed prior to the development of lightning jumps on shorter timescales (i.e., < 15 minutes).

However, this discussion goes beyond the timescale at which correlations are made in these analyses. The peak updraft speed and 10 m s^{-1} updraft volume are found to be higher than the fall speeds of ice hydrometeors responsible for electrification in thunderstorms. Ice crystals and graupel/small hail contribute to electrification of thunderstorms and their typical fall speeds have been found to be $\leq 10 \text{ m s}^{-1}$ (e.g., Dye et al. 1983, Dye et al. 1986, Musil et al. 1986, Musil and Smith 1989). The literature also shows that lightning propagation typically avoids regions of peak updraft speed and intense updraft volume due to lower concentrations of precipitation size ice and a lack of available charge (e.g., Wiens et al. 2005, Payne et al. 2010, Emersic et al. 2011, Calhoun et al. 2013, Kozlowski and Carey 2014). These regions are referred to as “lightning holes.” Therefore, the outstanding question remains; *why* do these intense updraft characteristics matter to rapid lightning production?

Data from the 10 April 2009 case in Schultz et al. (2015) provides the best observational evidence of the importance of 10 m s^{-1} updraft volume and peak updraft speed working in combination to influence the total flash rate. Figure 5 shows constant altitude plan position indicator (CAPPI) at 6 km and a north-south oriented cross section through the most intense part of this developing supercell 8 minutes prior to lightning jump occurrence at 1720 UTC. Flashes during this period of time are primarily initiating in regions of weaker updraft (e.g., $< 10 \text{ m s}^{-1}$). Much of the lightning activity is to the north or south of the

main updraft and contain convex hull-derived flash footprints⁶ $\geq 50 \text{ km}^2$. Figure 6 shows a north-south oriented cross section through the same supercell at 1739 UTC 9 minutes after two consecutive lightning jumps at 1728 and 1730 UTC. The highest density of flashes is now occurring above and along the sides of the core updraft region. The location observed to have the largest number of flashes also corresponds to the region where the smallest flash footprints are found. During this period of time, the 10 m s^{-1} updraft volume and peak updraft speed increase by over 100 km^3 and 20 m s^{-1} , respectively. Thus, it appears that the expansion of the 10 m s^{-1} updraft volume results in a larger three dimensional volume of weaker updraft and a larger interface between the updraft and downdraft regions. This leads to more frequent lightning flashes with smaller flash footprints in regions around the thunderstorm updraft. These regions near the updraft are known for turbulent motion (e.g. Knupp and Cotton 1982, Pantley and Lester 1990, Lane et al. 2003, Bedka et al. 2015, Behnke and Bruning 2015).

The measurements within this study are not at sufficient spatial and temporal resolution to examine this hypothesis beyond this inference. It is likely that the lightning jump is due to a combination of the increase in 10 m s^{-1} updraft volume (i.e., more cloud water, particle charging) and turbulence (i.e., smaller, more numerous charge regions; Bruning and MacGorman 2013); however, this hypothesis also relies on the ability of opposite charges to separate from each other in regions of higher turbulence (e.g., Bruning and MacGorman 2013).

⁶Flash footprint (i.e., approximate area the flash occupies in space) calculations are made in the same manner as Schultz et al. (2015) using the convex hull methodology outlined in Bruning and MacGorman (2013).

340 *b. The Less Definitive Role of Graupel Mass for Lightning Jumps*

341 Another outcome of this study is that changes in graupel mass are not shown to be sta-
 342 tistically robust indicators that separate jumps and non-jump increases in total flash rate.
 343 Figure 1 shows an increase in graupel mass during the 15 minutes prior to most increases
 344 in total flash rate. This indicates that graupel mass changes play a similar role for both
 345 jump and non-jump increases in total flash rate. Previous studies which show ice mass and
 346 total flash rates are well-correlated over longer periods of time (i.e., entire lifecycle of the
 347 storm) also provide plausibility to this hypothesis. Deierling et al. (2008)’s Figs. 11 and 12
 348 specifically illustrate that the same ice/graupel mass magnitude results in total flash rates
 349 which differ by as much as a factor of 10. This means that the relationship is not linear and
 350 one specific graupel mass does not result in one specific flash rate. Similarly, Schultz et al.
 351 (2015) shows that similar changes in graupel mass result in different flash rates and DFRDT
 352 values (e.g., their Table 1). Therefore, the rate of change of the graupel mass also is not
 353 directly related to the rate of change of the flash rate.

354

355 *c. Kinematic and Microphysical Characteristics of Severe Storms without Jumps*

356 The lightning jump algorithm in its current form will not be a stand alone warning
 357 algorithm. There are several scenarios where severe weather is produced and lightning pro-
 358 duction is small or non-existent (e.g., Butts 2006, Schultz et al. 2009, Schultz et al. 2011).

In fact, nearly 40% (64/161) of the missed severe weather events by the lightning jump in Schultz et al. (2011) were due to cold season and tropical cyclone storms that produce very little lightning. These environments mainly consisted of very little thermally buoyant energy (e.g., $\text{CAPE} \leq 500 \text{ J kg}^{-1}$) and strong 0-3 km wind shear (not shown).

The 39 thunderstorm dataset contains 6 thunderstorms that fit the low topped, cold season or tropical classification which also lack lightning jumps. All 6 of these storms are severe and produce hail, high winds or tornadoes. The median (mean) increase in graupel mass for these types of severe storms is $1.96 \times 10^7 \text{ kg}$ ($3.54 \times 10^7 \text{ kg}$), and the median trend in graupel mass for these 5 storms falls below the 25th percentile for trends in graupel mass prior to lightning jumps of $2.31 \times 10^7 \text{ kg}$ (Fig. 1). Mixed phase 10 m s^{-1} updraft volume growth and peak updraft speed intensification are also weak. The median (mean) 10 m s^{-1} updraft volume increase is 0 km^3 (15 km^3) for these types of severe storms. Furthermore, median (mean) increases in the peak mixed phase updraft speed are only on the order of 0.4 m s^{-1} (1.5 m s^{-1}) prior to their peak increase in total flash rate. Thus, there is a lack of mixed phase updraft growth or a total absence of 10 m s^{-1} updraft volume within this set of storms (3 of the 6 cases have a 10 m s^{-1} updraft volume of 0 km^3). Weaker magnitude changes in peak vertical velocity are also observed in these storms (Fig. 3). These weaker mixed phase kinematic properties limit the storm's potential to produce lightning and lightning jumps prior to severe weather occurrence.

The weak mixed phase updraft magnitudes and changes in magnitude observed in this study are similar to those found in other shallow severe storms in previous observational and modeling studies (e.g., McCaul and Weisman 1996, Cantrell 1995, Knupp et al. 1998, Eastin and Link 2009). This indicates that severe weather production does not always require ro-

bust mixed phase updrafts. This is why lightning trends in these types of storm may not always be useful for providing lead time on severe weather occurrence because of the limited size of the updraft or lack of strong mixed updraft speeds in cold season, low topped, or tropical cyclone severe thunderstorm environments.

5. Conclusions

The results of this work provide a comprehensive statistical evaluation for physical parameters which are hypothesized to modulate electrification and lightning in thunderstorms. A large dataset of 39 thunderstorms with 214-fifteen minute analysis windows are used to assess trends in mixed phase graupel mass, updraft volume and updraft speed prior to lightning jumps and other non-jump increases in total flash rate. The following conclusions were made from this analysis:

- Graupel mass is not observed to be a statistically significant discriminator between lightning jumps (i.e., 2+ sigma-level) and non-jump (i.e., 0-2 sigma-level) increases in total flash rate. The one-tailed p-value for the independence test of the jump and non-jump distributions is $p=0.096$.
- The change in 5 m s^{-1} updraft volume is also not observed to be statistically significant discriminator between lightning jumps and non-jump increases in total flash rate. The

one-tailed p-value for the independence test of the jump and non-jump distributions is $p=0.093$.

- Larger increases in 10 m s^{-1} updraft volume are observed for lightning jumps versus those observed with non-jump increases in total flash rate ($p=0.0234$). The median change in 10 m s^{-1} updraft volume for jump and non-jump categories is 62 km^3 and 16 km^3 , respectively.

- Larger magnitude increases in peak updraft speed are observed for lightning jumps versus those observed with non-jump increases in total flash rate ($p=5.0 \times 10^{-4}$). The median change in maximum updraft speed is 5 m s^{-1} and 1 m s^{-1} for jump and non-jump increases, respectively (Fig. 3).

- Very little difference is found in the timing between peak increase in each of the three kinematic/microphysical parameters (mixed phase graupel mass, 10 m s^{-1} updraft volume and peak maximum updraft speed) relative to the time of the total flash rate increase. In general, growth occurs between 4 and 13 minutes in advance of most flash rate increases.

- A sample of 6 severe thunderstorms that did not produce lightning jumps demonstrate that the main characteristic lacking in these storms is mixed phase updraft. These

storms lack significant changes in 10 m s^{-1} updraft volume and the magnitude of the peak updraft speed in the mixed phase region during their largest increases in total flash rate.

These strong statistical results support the use of lightning jumps to infer changes in stronger updraft characteristics in thunderstorms. Often these physical parameters are not readily available in operational datasets, and thus the lightning data can provide some indication on the trend of the mixed phase updraft (growing vs weakening). Future work will need to demonstrate the physical connections between mixed phase updraft growth and severe weather production in thunderstorms.

Acknowledgments.

The authors would like to acknowledge Dr. Steven J. Goodman and GOES-R Risk Reduction Research funding for support of this research. C. Schultz would like to acknowledge support from the NASA Pathways Intern Program at Marshall Space Flight Center, namely Julie Clift and Christopher Randall. The authors are; thankful for technical support with radar data processing from Lamont Bain, Retha Mecikalski, and Danielle Kozlowski for parts of the June 11 and April 10 events. Furthermore, productive conversations with Drs. Themis Chronis, Phil Bitzer, Hugh Christian, Walt Petersen, Kristin Calhoun and Eric Bruning benefited the outcomes of this research. We also gratefully acknowledge the technical support for maintenance of the operational instrumentation, namely Dustin Phillips, Patrick Gatlin,

Chris Phillips for the maintenance of the ARMOR radar. The authors would also like to recognize Jeff Bailey and Blair Breitreiter for the continued maintenance of the North Alabama Lightning Mapping Array. Finally, the authors would like to thank Editor Dr. Paul Markowski and two anonymous reviewers for their helpful comments which improved the content and technical writing of this manuscript.

APPENDIX

Appendix A

a. 2σ Lightning Jump Algorithm

Although the lightning jump algorithm has been described in previous work (e.g., Schultz et al. 2009, Schultz et al. 2011, Chronis et al. 2015) it is good to review the formulation of the algorithm for reference to this work. The primary source of lightning data for this algorithm has been lightning mapping arrays with the goal of ultimately utilizing GLM once GOES-R data are operationally available.

The algorithm starts with 14 minutes of total lightning data which has been assigned to a specific thunderstorm. For this example, t_0 is the most recent minute of data, and $t-13$ is the oldest minute of data. First, 1 minute flash rates are combined to produce an average

flash rate every 2 minutes. For example, the average flash rate for time t_0 and time $t-1$ is,

$$FR_{avg}(t_0)(\text{flashes min}^{-1}) = \frac{FR_{t_0} + FR_{t-1}}{2 \text{ minutes}}, \quad (\text{A1})$$

while the average flash rate for times $t-12$ and $t-13$ would be,

$$FR_{avg}(t-12)(\text{flashes min}^{-1}) = \frac{FR_{t-12} + FR_{t-13}}{2 \text{ minutes}}. \quad (\text{A2})$$

464

Now there are a total of 7 1-minute average flash rates: $FR_{avg}(t_0)$, $FR_{avg}(t-2)$, $FR_{avg}(t-4)$, $FR_{avg}(t-6)$, $FR_{avg}(t-8)$, $FR_{avg}(t-10)$, $FR_{avg}(t-12)$. Next, subsequent FR_{avg} times are subtracted from each other to obtain the rate of change of the total flash rate, or more commonly known as DFRDT. For the rate of change in the flash rate between $FR_{avg}(t_0)$ and $FR_{avg}(t-2)$ the equation would be,

$$DFRDT_{t_0} = \frac{FR_{avg}(t_0) - FR_{avg}(t-2)}{2 \text{ minutes}} = DFRDT(\text{flashes min}^{-2}), \quad (\text{A3})$$

while for $FR_{avg}(t-10)$ and $FR_{avg}(t-12)$ the equation would be,

$$DFRDT_{t-10} = \frac{FR_{avg}(t-10) - FR_{avg}(t-12)}{2 \text{ minutes}} = DFRDT(\text{flashes min}^{-2}). \quad (\text{A4})$$

471

Now there are a total of 6 DFRDT values for the algorithm to use to identify a lightning jump ($DFRDT_{t_0}$, $DFRDT_{t-2}$, $DFRDT_{t-4}$, $DFRDT_{t-6}$, $DFRDT_{t-8}$, $DFRDT_{t-10}$). $DFRDT_{t_0}$ is the current rate of change of the total flash rate in the storm, while $DFRDT_{t-2}$, $DFRDT_{t-4}$, $DFRDT_{t-6}$, $DFRDT_{t-8}$ and $DFRDT_{t-10}$ are used to calculate the standard deviation of the rate of change of the total flash rate in the storm between time $t-2$ up to (and not including) $t-14$. The result is the sigma-level calculation found in Eqn. 2. A sigma-level

478 value ≥ 2 identifies a lightning jump, while a sigma-level value < 2 is identified as a non-
479 jump increase in the total flash rate. This representation of the 2σ lightning jump algorithm
480 provides users with more information than the previous algorithm (i.e., a yes/no answer
481 that the 2σ lightning jump threshold has been exceeded) by allowing the user to determine
482 how far above or below any increase in total flash rate is relative to the dynamic 2σ threshold.

483

REFERENCES

- 486 Armijo, L., 1969: A theory for the determination of wind and precipitation velocities with
 487 Doppler radars. *J. Atmos. Sci.*, **26**, 570–573.
- 488 Bedka, K. M., C. Wang, R. Rogers, L. D. Carey, W. Feltz, and J. Kanak, 2015: Examining
 489 deep convective cloud evolution using total lightning, WSR-88D, and GOES-14 Super
 490 Rapid Scan datasets. *Wea. Forecasting*, doi:http://dx.doi.org/10.1175/WAF-D-14-00062.
 491 1.
- 492 Behnke, S. A. and E. C. Bruning, 2015: Changes to the turbulent kinematics of a volcanic
 493 plume inferred from lightning data. *Geophys. Res. Lett.*, **42**, 4232–4239.
- 494 Brandes, E. A., 1977: Flow in severe thunderstorms observed by dual-Doppler radar. *Mon.*
 495 *Wea. Rev.*, **105**, 113–120.
- 496 Bringi, V. N., T. D. Keenan, and V. Chandrasekar, 2001: Correcting C-band radar reflec-
 497 tivity and differential reflectivity data for rain attenuation: A self-consistent method with
 498 constraints. *IEEE Trans. On Geo. and Rem. Sens.*, **39**, 1906–1915.
- 499 Bringi, V. N., K. R. Knupp, A. Detwiler, L. Liu, I. J. Caylor, and R. A. Black, 1997: Evo-
 500 lution of a Florida thunderstorm during the Convection and Precipitation/Electrification
 501 Experiment: The case of 9 August 1991. *Mon. Wea. Rev.*, **125**, 2131–2160.
- 502 Bruning, E. C. and D. M. MacGorman, 2013: Theory and observations of controls on light-
 503 ning flash spectra. *J. Atmos. Sci.*, **70**, 4012–4029.

504 Butts, D., 2006: *An examination of the relationship between cool season tornadoes and*
505 *cloud-to-ground lightning flashes*. MS Thesis, Texas A and M University, 109 pp.

506 Byers, H. R. and R. R. Braham, 1949: *The Thunderstorm*. U. S. Government Printing Office,
507 287 pp.

508 Calhoun, K. M., 2015: Forecaster use of total lightning data for short-term forecasts and
509 warnings in the Hazardous Weather Testbed. *7th Conf. on Meteorological Applications of*
510 *Lightning Data*, Phoenix, AZ.

511 Calhoun, K. M., D. R. MacGorman, C. L. Ziegler, and M. I. Biggerstaff, 2013: Evolution of
512 lightning activity and storm charge relative to dual-Doppler analysis of a high-precipitation
513 supercell storm. *Mon. Wea. Rev.*, **141**, 2199–2223.

514 Cantrell, L. E., Jr., 1995: *The Role of Vertical Buoyancy Distribution in Simulated Low-*
515 *Topped Supercells*. M.S. Thesis, Texas A & M University, 135 pp.

516 Carey, L. D., W. J. Koshak, H. Peterson, and R. M. Mecikalski, 2016: The kinematic and
517 microphysical control of lightning rate, extent, and NO_x production. *J. Geophys. Res.*,
518 **121**, 7975–7989.

519 Carey, L. D. and S. A. Rutledge, 1996: A multiparameter radar case study of the micro-
520 physical and kinematic evolution of a lightning producing storm. *Meteorol. Atmos. Phys.*,
521 **59**, 33–64.

522 Chronis, T., L. D. Carey, C. J. Schultz, E. V. Schultz, K. M. Calhoun, and S. J. Goodman,
523 2015: Exploring lightning jump characteristics. *Wea. Forecasting*, Accepted, in publica-
524 tion.

525 Crum, T. D. and R. L. Alberty, 1993: The WSR-88D and the WSR-88D Operational Support
526 Facility. *Bull. Amer. Meteor. Soc.*, **74**, 1669–1687.

527 Davies-Jones, R. P., 1979: Dual-Doppler radar coverage area as a function of measurement
528 accuracy and spatial resolution. *J. Appl. Meteor.*, **18**, 1229–1233.

529 Deierling, W. and W. A. Petersen, 2008: Total lightning activity as an indicator of updraft
530 characteristics. *J. Geophys. Res.*, **113**, doi:10.1029/2007JD009598.

531 Deierling, W., W. A. Petersen, J. Latham, S. Ellis, and H. J. Christian, 2008: The relation-
532 ship between lightning activity and ice fluxes in thunderstorms. *J. Geophys. Res.*, **113**,
533 doi:10.1029/2007JD009700.

534 Dixon, M. and G. Wiener, 1993: TITAN: Thunderstorm Identification, Tracking Analysis
535 and Nowcasting-A radar-based methodology. *J. Atmos. Ocean Tech.*, **10**, 785–797.

536 Dye, J. E. and Coauthors, 1986: Early electrification and precipitation development in a
537 small, isolated Montana cumulonimbus. *J. Geophys. Res.*, **91**, 1231–1247.

538 Dye, J. E., B. E. Martner, and L. J. Miller, 1983: Dynamical-microphysical evolution of a
539 convective storm in a weakly-sheared environment. Part I: Microphysical observations and
540 interpretation. *J. Atmos. Sci.*, **40**, 12083–2096.

541 Dye, J. E., W. P. Winn, J. J. Jones, and D. W. Breed, 1989: The electrification of New
542 Mexico thunderstorms. 1. Relationship between precipitation development and the onset
543 of electrification. *J. Geophys. Res.*, **94**, 8643–8656.

- Eastin, M. D. and M. C. Link, 2009: Minature supercells in an offshort outer rainband of Hurricane Ivan (2004). *Mon. Wea. Rev.*, **137**, 2081–2104.
- Emersic, C., P. L. Heinselman, D. R. MacGorman, and E. C. Bruning, 2011: Lightning activity in a hail-producing storm observed with phased array radar. *Mon. Wea. Rev.*, **139**, 1809–1824, doi:10.1175/2010MWR3574.1.
- Gatlin, P. N. and S. J. Goodman, 2010: A total lightning trending algorithm to identify severe thunderstorms. *J. Atmos. Oceanic Technol.*, **27**, 3–22.
- Goodman, S. J., D. E. Buechler, P. D. Wright, and W. D. Rust, 1988: Lightning and precipitation history of a microburst-producing storm. *Geophys. Res. Lett.*, **15**, 1185–1188.
- Goodman, S. J. and Coauthors, 2005: The North Alabama Lightning Mapping Array: Recent severe storm observations and future prospects. *Atmos. Res.*, **76**, 423–437.
- Goodman, S. J. and Coauthors, 2013: The GOES-R Geostationary Lightning Mapper (GLM). *Atmos. Res.*, **125–126**, 34–49.
- Heymsfield, A. J. and K. M. Miller, 1988: Water vapor and ice mass transported into the anvils of CCOPE thunderstorms: Comparison with storm influx and rainout. *J. Atmos. Sci.*, **45**, 3501–3514.
- Johnson, E. V., 2009: *Behavior of Lightning and Updrafts for Severe and Non Severe Thunderstorms in Northern Alabama*. M.S. Thesis, University of Alabama-Huntsville, 70 pp.
- Knupp, K. R. and Coauthors, 2014: Meteorological overview of the devastating 27 April

- 2011 tornado outbreak. *Bull. Amer. Meteor. Soc.*, **95**, 1041–1062, doi:<http://dx.doi.org/10.1175/BAMS-D-11-00229.1>.
- Knupp, K. R. and W. R. Cotton, 1982: An intense, quasi-steady thunderstorm over mountainous terrain: Part III: Doppler radar observations of the turbulent structure. *J. Atmos. Sci.*, **39**, 359–368.
- Knupp, K. R., J. R. Stalker, and E. W. McCaul, 1998: An observational and numerical study of a mini-supercell storm. *Atmos. Res.*, **49** (1), 35–63.
- Koshak, W. J. and Coauthors, 2004: North Alabama Lightning Mapping Array (LMA): VHF source retrieval algorithm and error analysis. *J. Atmos. Ocean. Tech.*, **21**, 543–558.
- Kozlowski, D. M. and L. D. Carey, 2014: An analysis of lightning holes in Northern Alabama severe storms using a lightning mapping array and dual-polarization radar. *Preprints, 5th Inter. Lightning Meteorology Conf.*, Tuscon, AZ, <http://www.vaisala.com/en/events/ildcilmc/Pages/ILDC-2014-archive.aspx>.
- Kuhlman, K. M., C. L. Zeigler, E. R. Mansell, D. R. MacGorman, and J. M. Straka, 2006: Numerically simulated electrification and lightning of the 29 June 2000 STEPS supercell storm. *Mon. Wea. Rev.*, **134**, 2734–2757.
- Lane, T. P., R. D. Sharman, T. L. Clark, and H. M. Hsu, 2003: An investigation of turbulence generation mechanisms above deep convection. *J. Atmos. Sci.*, **60**, 1297–1321.
- Lang, T. J. and S. A. Rutledge, 2002: Relationships between convective storm kinematics, precipitation, and lightning. *Mon. Wea. Rev.*, **130**, 2492–2506.

583 Matejka, T. and D. L. Bartels, 1998: The accuracy of vertical air velocities from Doppler
584 radar data. *Mon. Wea. Rev.*, **92**, 92–117.

585 McCaul, E. W., S. J. Goodman, K. M. LaCasse, and D. J. Cecil, 2009: Forecasting lightning
586 threat using cloud-resolving model simulations. *Weather and Forecasting*, **24** (3), 709–729,
587 doi:10.1175/2008WAF2222152.1.

588 McCaul, E. W., Jr. and M. L. Weisman, 1996: Simulations of shallow supercell storms in
589 landfalling hurricane environments. *Mon. Wea. Rev.*, **124**, 408–429.

590 Mecikalski, R. M., A. L. Bain, and L. D. Carey, 2015: Radar and lightning observations of
591 deep moist convection across Northern Alabama during DC3: 21 May 2012. *Mon. Wea.*
592 *Rev.*, **143**, 2774–2794.

593 Mohr, C. G., L. J. Miller, R. L. Vaughn, and H. W. Frank, 1986: On the merger of mesoscale
594 datasets into a common Cartesian format for efficient and synthetic analysis. *J. Atmos.*
595 *Oceanic. Technol.*, **3**, 141–161.

596 Musil, D. J., A. J. Heymsfield, and P. L. Smith, 1986: Microphysical characteristics of a
597 well-developed weak echo region in a High Plains supercell thunderstorm. *J. Clim. and*
598 *Appl. Meteor.*, **25**, 1037–1051.

599 Musil, D. J. and P. L. Smith, 1989: Interior characteristics at mid-levels of thunderstorms
600 in the Southeastern United States. *Atmos. Res.*, **24**, 149–167.

601 O’Brien, J. J., 1970: Alternative solutions to the classical vertical velocity problem. *J. Appl.*
602 *Meteor.*, **9**, 197–203.

603 Oye, D. and M. Case, 1995: REORDER: A Program for Gridding Radar Data. Installa-
604 tion and User Manual for the UNIX Version. NCAR Atmospheric Technology Division,
605 Boulder, CO, 19 pp.

606 Oye, D., C. Mueller, and S. Smith, 1995: Software for radar translation, visualization, editing
607 and interpolation. *Preprints, 27th Conf. on Radar Meteorology*, 359–361, Vail, CO, Amer.
608 Met. Soc.

609 Pantley, K. C. and P. F. Lester, 1990: Observations of severe turbulence near thunderstorm
610 tops. *J. Appl. Meteor.*, **60**, 1171–1179.

611 Payne, C. D., T. J. Schuur, D. R. MacGorman, M. I. Biggerstaff, K. M. Kuhlman, and W. D.
612 Rust, 2010: Polarimetric and electrical characteristics of a lightning ring in a supercell
613 storm. *Mon. Wea. Rev.*, **138**, 2405–2425.

614 Ray, P. S., C. L. Ziegler, W. Bumgarner, and R. J. Serafin, 1980: Single and multiple-Doppler
615 radar observations of tornadic storms. *Mon. Wea. Rev.*, **108**, 1607–1625.

616 Rudlosky, S. D. and H. E. Fuelberg, 2013: Documenting storm severity in the Mid-Atlantic
617 region using lightning and radar information. *Mon. Wea. Rev.*, **141**, 3186–3202, doi:10.
618 1175/MWR-D-12-00287.1.

619 Saunders, C. P. R., H. Bax-Norman, C. Emersic, E. E. Avila, and N. E. Castellano, 2006:
620 Laboratory studies of the effect of cloud conditions on graupel/crystal charge transfer in
621 thunderstorm electrification. *Quart. J. Roy. Meteor. Soc.*, **132**, 2653–2673.

622 Schultz, C. J., L. D. Carey, E. V. Schultz, and R. L. Blakeslee, 2015: Insight into the

physical and dynamical processes that control rapid increases in total flash rate. *Mon. Wea. Forecasting*, **30**, 1591–1621.

Schultz, C. J. and Coauthors, 2012: Dual-polarization tornadic debris signatures Part I: Examples and utility in an operational setting. *Electronic J. Operational Meteor.*, **13**, 120–137.

Schultz, C. J., W. A. Petersen, and L. D. Carey, 2009: Preliminary development and evaluation of lightning jump algorithms for the real-time detection of severe weather. *J. Appl. Meteor.*, **48**, doi:10.1175/2009JAMC2237.1.

Schultz, C. J., W. A. Petersen, and L. D. Carey, 2011: Lightning and severe weather: A comparison between total and cloud-to-ground lightning trends. *Wea. Forecasting*, **26**, 744–755, doi:10.1175/WAF-D-10-05026.1.

Takahashi, T., 1978: Riming electrification as a charge generation mechanism in thunderstorms. *J. Atmos. Sci.*, **35**, 1536–1548.

Tessendorf, S. A., L. J. Miller, K. C. Wiens, and S. A. Rutledge, 2005: The 29 June 2000 supercell observed during STEPS. Part I: Kinematics and microphysics. *JAS*, **62**, 4127–4150.

Tuttle, J. D., V. N. Bringi, H. D. Orville, and F. J. Kopp, 1989: Multiparameter radar study of a microburst - comparison with model results. *J. Atmos. Sci.*, **46**, 601–620.

Vivekanandan, J., D. S. Zrnic, S. M. Ellis, R. Oye, A. V. Ryzhkov, and J. Straka, 1999: Cloud microphysics retrieval using S-band dual-polarization radar measurements. *Bull. Amer. Met. Soc.*, **80**, 381–388.

644 Wiens, K. C., S. A. Rutledge, and S. A. Tessendorf, 2005: The 29 June 2000 supercell
645 observed during steps. Part II: Lightning and charge structure. *J. Atmos. Sci.*, **62**, 4151–
646 4177.

647 Wilks, D. S., 1995: *Statistical Methods in the Atmospheric Sciences*. Academic Press, 467
648 pp.

649 Williams, E. R. and Coauthors, 1999: The behavior of total lightning activity in severe
650 Florida thunderstorms. *Atmos. Res.*, **51**, 245–265.

651 Williams, E. R., M. E. Weber, and R. E. Orville, 1989: The relationship between lightning
652 type and convective state of thunderclouds. *J. Geophys. Res.*, **94**, 13 213–13 220.

653 Witt, A., M. D. Eilts, G. J. Stumpf, J. T. Johnson, E. D. Mitchell, and K. W. Thomas, 1998:
654 An enhanced hail detection algorithm for the WSR-88D. *Wea. Forecasting*, **13**, 286–303.

655 Workman, E. J. and S. E. Reynolds, 1949: Electrical activity as related to thunderstorm cell
656 growth. *Bull. Amer. Meteor. Soc.*, **30**, 142–144.

657 List of Tables

| | | | |
|-----|---|---------------------------------------------------------------------------------------------------|----|
| 658 | 1 | Dates, number of storms, storm type and the number of storms from each day | |
| 659 | | used in this analysis. | 35 |
| 660 | 2 | Z-scores and p-values using Wilcoxon-Mann-Whitney Rank Sum Testing be- | |
| 661 | | tween the 0-2 and 2+ sigma-level categories for Graupel Mass Change (kg), | |
| 662 | | 5 and 10 m s ⁻¹ updraft volume change (km ³) and maximum vertical velocity | |
| 663 | | change (m s ⁻¹) | 36 |

TABLE 1. Dates, number of storms, storm type and the number of storms from each day used in this analysis.

| Location | Number | Type | Jump | No Jump |
|-------------------|--------|------------|------|---------|
| 3 May 2006 | 1 | multicell | 1 | 0 |
| 19 July 2006 | 2 | multicell | 2 | 0 |
| 3 April 2007 | 3 | supercell | 2 | 1 |
| 4 April 2007 | 1 | QLCS | 1 | 0 |
| 1 June 2007 | 4 | multicell | 0 | 4 |
| 7 July 2007 | 2 | multicell | 2 | 0 |
| 17 August 2007 | 6 | multicell | 5 | 1 |
| 14 September 2007 | 1 | tropical | 0 | 1 |
| 10 April 2009 | 3 | supercell | 3 | 0 |
| 13 April 2009 | 1 | low topped | 0 | 1 |
| 21 January 2010 | 2 | low topped | 1 | 1 |
| 12 March 2010 | 1 | QLCS | 1 | 0 |
| 26 October 2010 | 3 | supercell | 0 | 3 |
| 27 April 2011 | 1 | supercell | 1 | 0 |
| 18 May 2012 | 1 | multicell | 1 | 0 |
| 21 May 2012 | 1 | multicell | 0 | 1 |
| 11 June 2012 | 4 | multicell | 0 | 4 |
| 14 June 2012 | 2 | multicell | 0 | 2 |

TABLE 2. Z-scores and p-values using Wilcoxon-Mann-Whitney Rank Sum Testing between the 0-2 and 2+ sigma-level categories for Graupel Mass Change (kg), 5 and 10 m s⁻¹ updraft volume change (km³) and maximum vertical velocity change (m s⁻¹)

| | Graupel Mass | 5 m s ⁻¹ | 10 m s ⁻¹ | MaxVV |
|----------------------|--------------|---------------------|----------------------|----------------------|
| Z-Score | 1.065 | 1.323 | 1.987 | 3.286 |
| p-value (one tailed) | 0.096 | 0.093 | 0.0234 | 5.0×10^{-4} |

List of Figures

- 1 Box plots of storm graupel mass change (kg) versus the sigma-level of the subsequent increase in total flash rate. Data from non-jump increases in total flash rates are in blue (i.e., 0-2 sigma-level), while data from lightning jump events are in orange. Median, 25th, and 75th changes are to the right of each box, and the population size of each bin is on the left. “X” marks indicate the individual data points within each sigma-level category. 39
- 2 Same as Fig. 1, but for storm 5 m s⁻¹ (Panel A) and 10 m s⁻¹ (Panel B) updraft volume change (km³) versus the sigma-level of the subsequent increase in total flash rate. 40
- 3 Same as Fig. 1, but for the change in peak updraft speed (m s⁻¹) versus the sigma-level of the subsequent increase in total flash rate. 41
- 4 Same as Fig. 1, but for the timing of the peak increase in graupel mass (Panel A), 10 m s⁻¹ updraft volume (Panel B) and maximum updraft updraft speed (Panel C) minus the time of flash rate increase distributed versus the sigma-level of the subsequent increase in total flash rate. 42

- 5 Reflectivity, updraft velocity, flash extent density and mean flash footprint
prior to lightning jump occurrence in a storm transitioning from multicell to
supercell on 10 April 2009. Panel A is a CAPPI of reflectivity at 6 km with
reflectivity (shaded every 5-dB starting at 5-dBZ, velocity (black contours in
 10 m s^{-1} increments starting at 10 m s^{-1}) and lightning flash origin (black
dots within 2 minutes of radar volume time) are overlaid. The gray dashed
rectangle represents the region which lightning data for flash extent density
and mean flash footprint are calculated from in Panels B and C. Panel B is
flash extent density (flashes km^{-2}) in $1 \text{ km} \times 1 \text{ km}$ bins within 2 minutes of
radar volume start time with reflectivity from ARMOR (solid black contours
every 10-dB, starting at 10-dBZ) and vertical velocity (blue contours starting
at 5 m s^{-1} , then in 10 m s^{-1} increments after 10 m s^{-1}) overlaid. Panel C is
mean flash footprint (km^2) within 2 minutes of radar volume start time with
with reflectivity from ARMOR (solid black contours every 10-dB, starting at
10-dBZ) and vertical velocity (blue dashed contours starting at 5 m s^{-1} , then
in 10 m s^{-1} increments after 10 m s^{-1}) overlaid. 43
- 6 Same as Fig. 5 but for 1739 UTC on 10 April 2009. 44

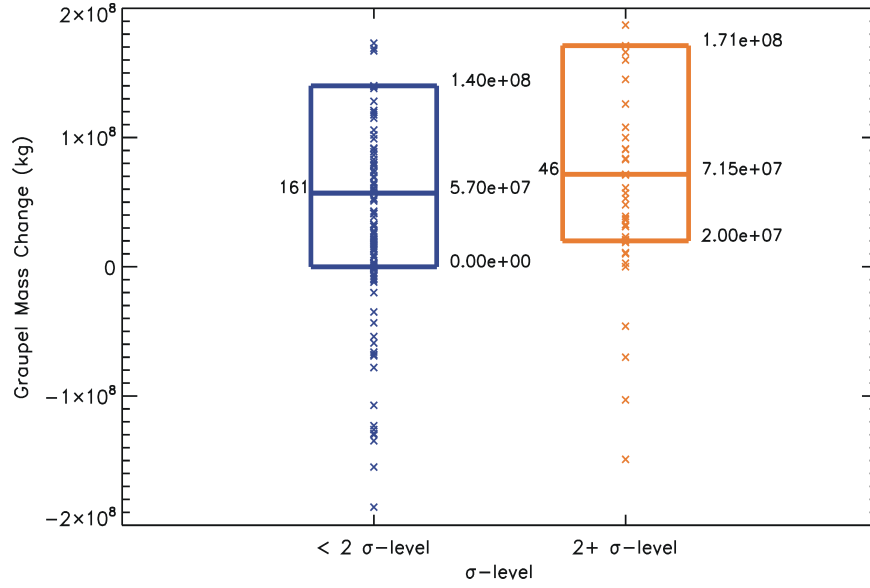


FIG. 1. Box plots of storm graupel mass change (kg) versus the sigma-level of the subsequent increase in total flash rate. Data from non-jump increases in total flash rates are in blue (i.e., 0-2 sigma-level), while data from lightning jump events are in orange. Median, 25th, and 75th changes are to the right of each box, and the population size of each bin is on the left. “X” marks indicate the individual data points within each sigma-level category.

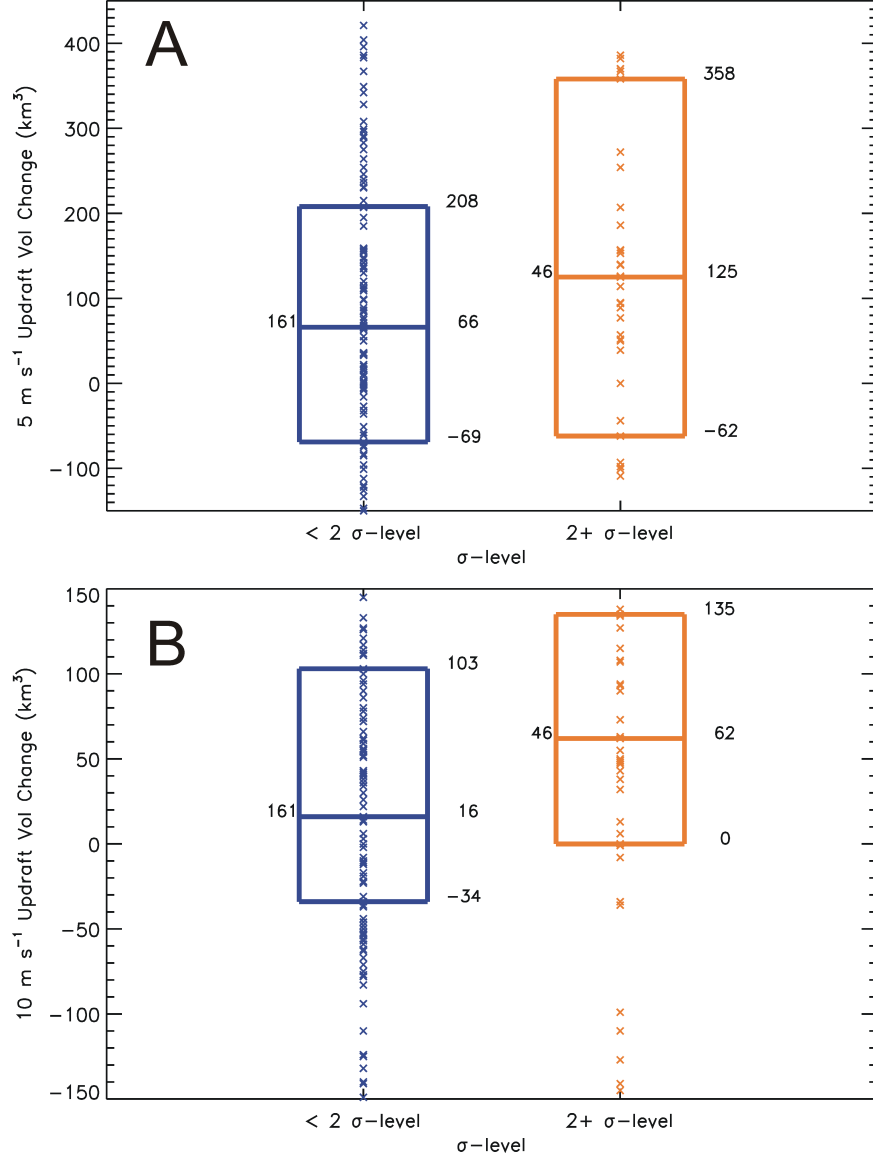


FIG. 2. Same as Fig. 1, but for storm 5 m s⁻¹ (Panel A) and 10 m s⁻¹ (Panel B) updraft volume change (km³) versus the sigma-level of the subsequent increase in total flash rate.

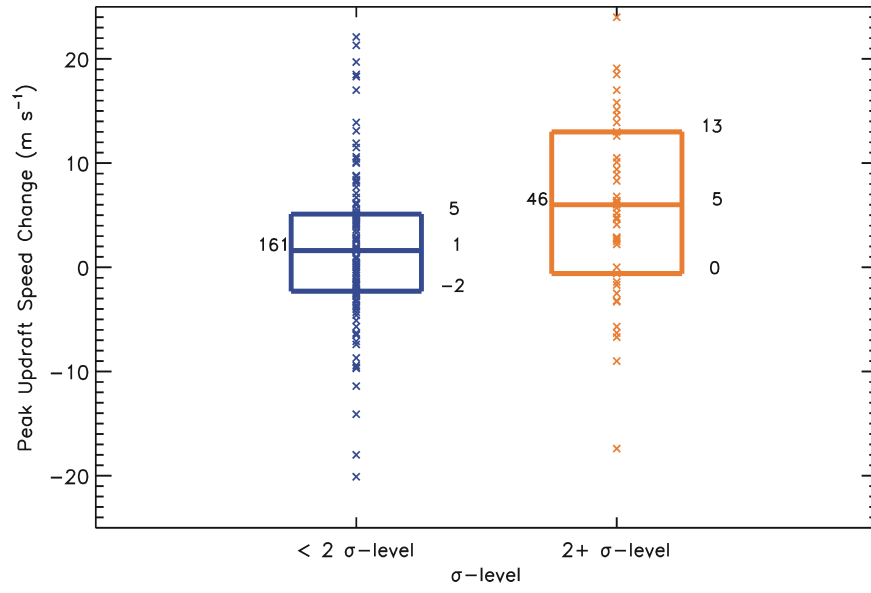


FIG. 3. Same as Fig. 1, but for the change in peak updraft speed (m s^{-1}) versus the sigma-level of the subsequent increase in total flash rate.

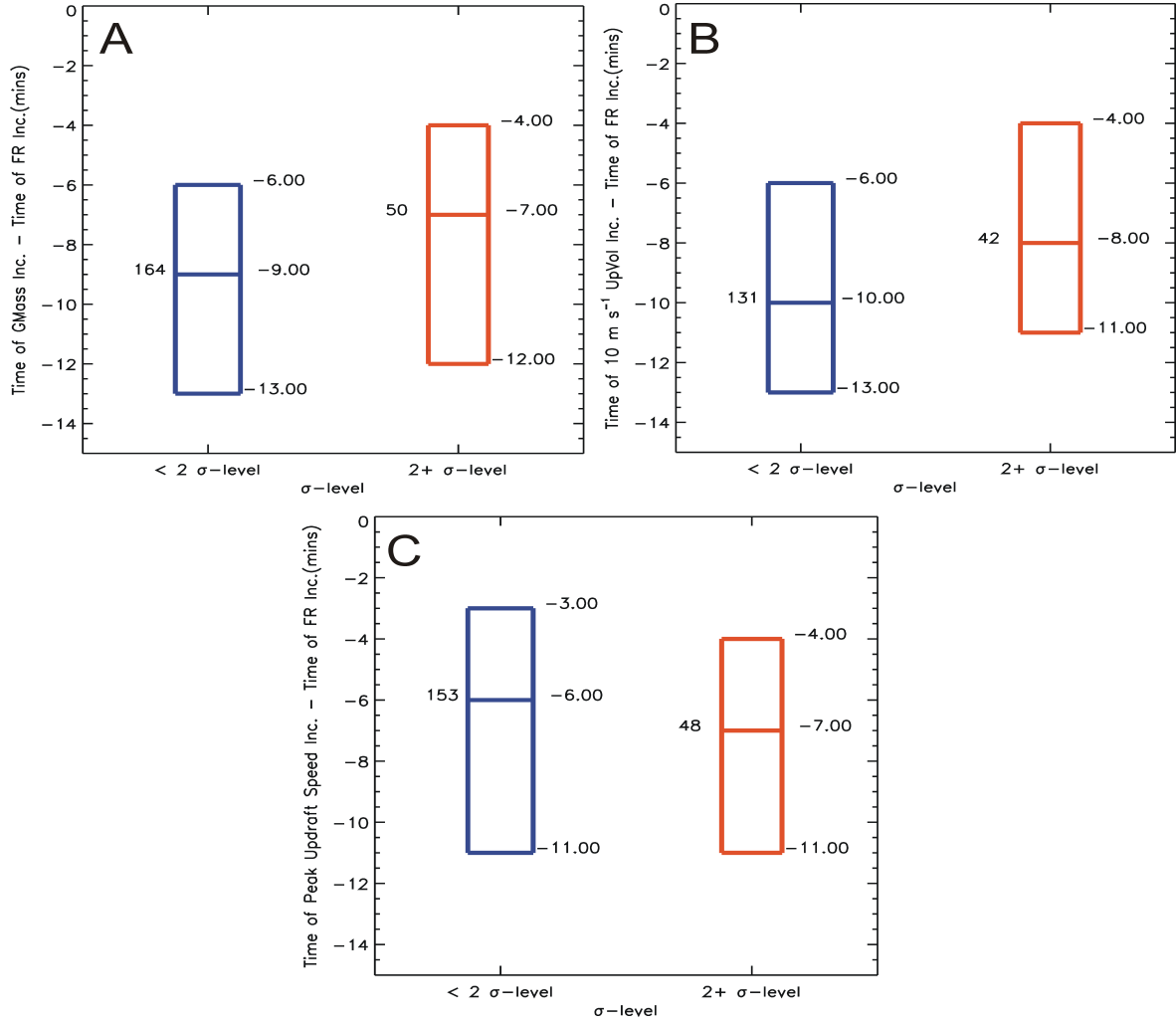


FIG. 4. Same as Fig. 1, but for the timing of the peak increase in graupel mass (Panel A), 10 m s^{-1} updraft volume (Panel B) and maximum updraft updraft speed (Panel C) minus the time of flash rate increase distributed versus the sigma-level of the subsequent increase in total flash rate.

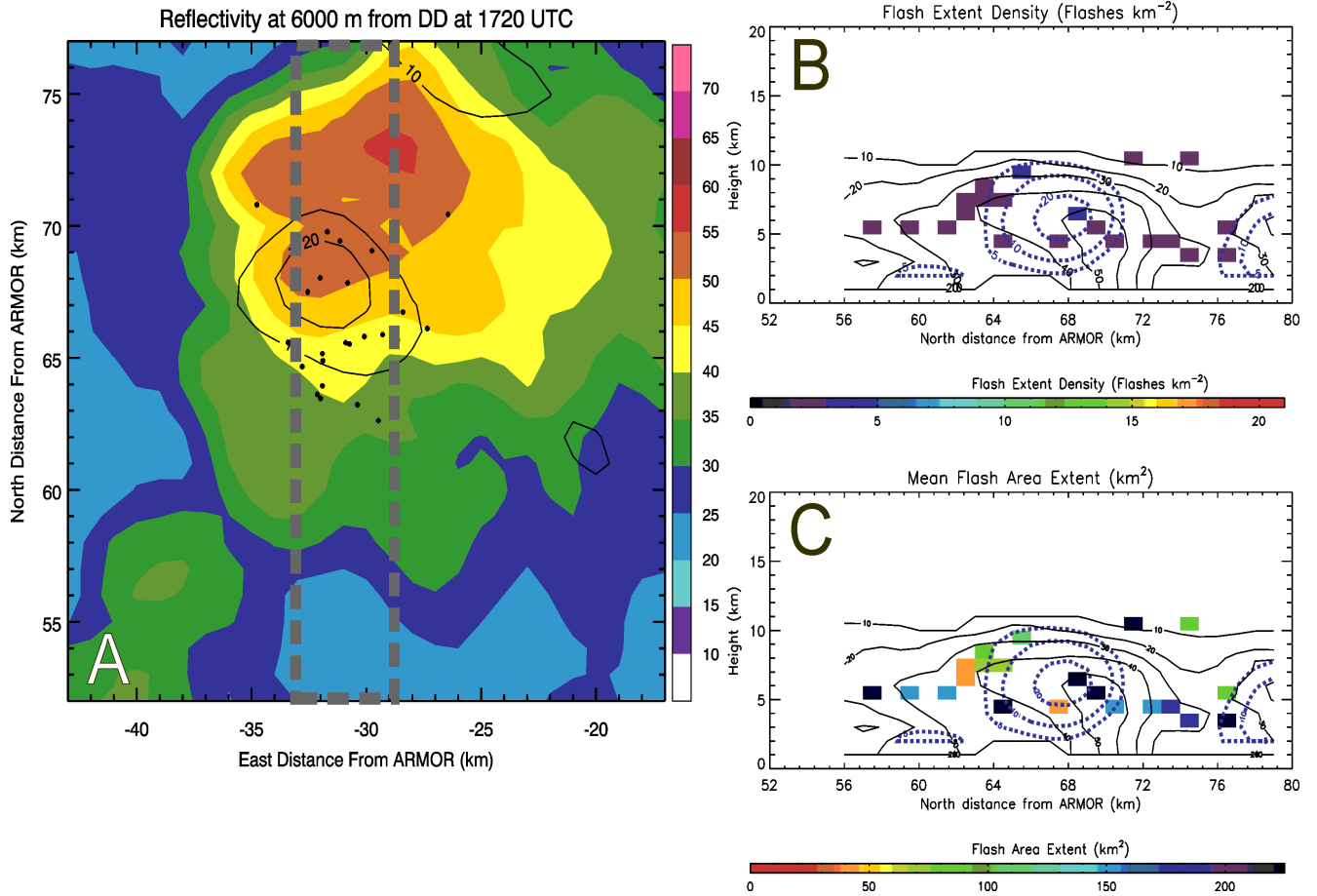


FIG. 5. Reflectivity, updraft velocity, flash extent density and mean flash footprint prior to lightning jump occurrence in a storm transitioning from multicell to supercell on 10 April 2009. Panel A is a CAPPI of reflectivity at 6 km with reflectivity (shaded every 5-dB starting at 5-dBZ, velocity (black contours in 10 m s^{-1} increments starting at 10 m s^{-1}) and lightning flash origin (black dots within 2 minutes of radar volume time) are overlaid. The gray dashed rectangle represents the region which lightning data for flash extent density and mean flash footprint are calculated from in Panels B and C. Panel B is flash extent density (flashes km^{-2}) in $1 \text{ km} \times 1 \text{ km}$ bins within 2 minutes of radar volume start time with reflectivity from ARMOR (solid black contours every 10-dB, starting at 10-dBZ) and vertical velocity (blue contours starting at 5 m s^{-1} , then in 10 m s^{-1} increments after 10 m s^{-1}) overlaid. Panel C is mean flash footprint (km^2) within 2 minutes of radar volume start time with with reflectivity from ARMOR (solid black contours every 10-dB, starting at 10-dBZ) and vertical velocity (blue dashed contours starting at 5 m s^{-1} , then in 10 m s^{-1} increments after 10 m s^{-1}) overlaid.

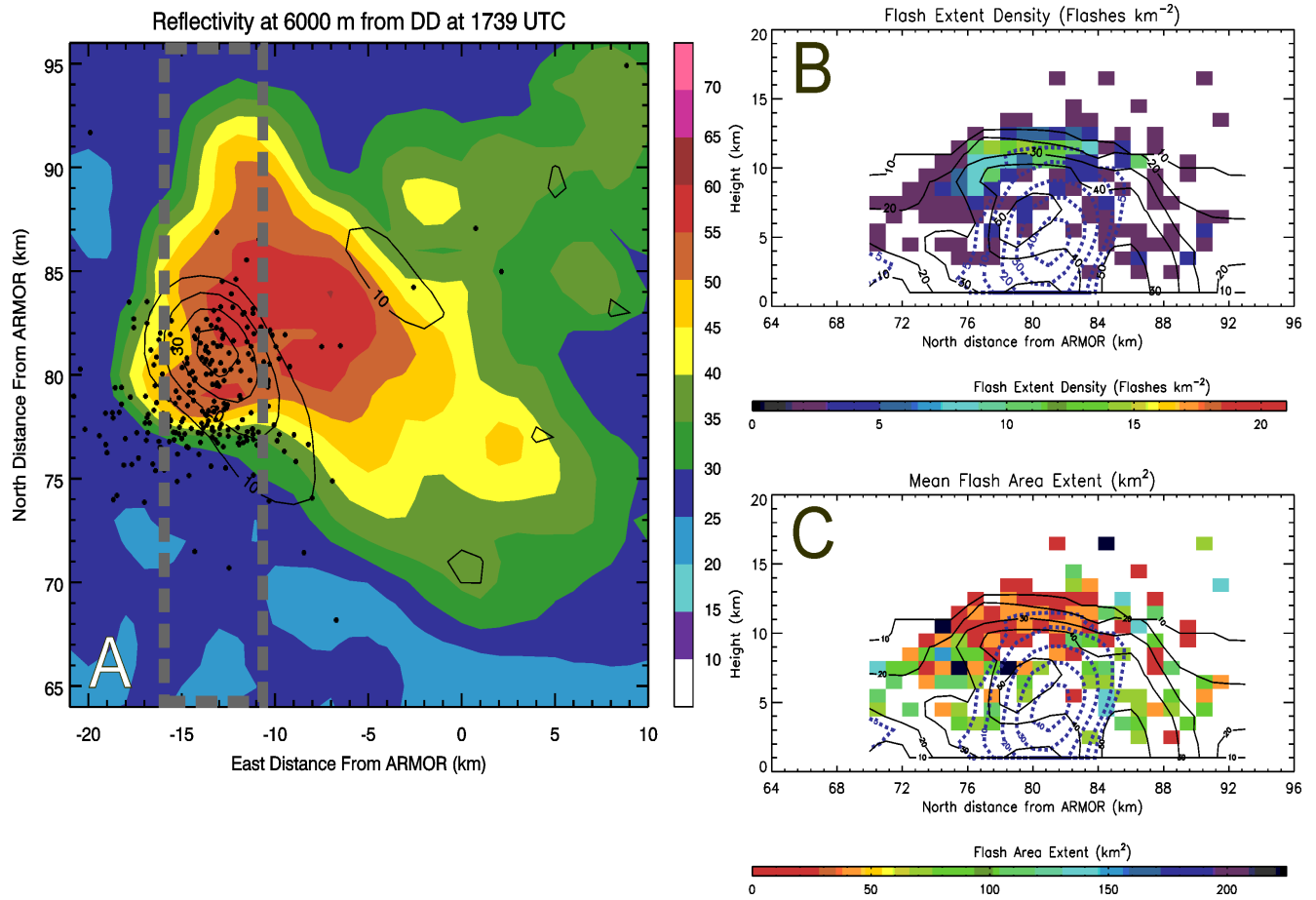


FIG. 6. Same as Fig. 5 but for 1739 UTC on 10 April 2009.